High-resolution simulations resolve three-dimensional evolution of barotropic frontal instabilities in mature cyclones. Variations in deformation along cold front explain simulated behavior.

Barotropic Instability of a Cyclone Core at Kilometer-Scale Resolution[1]

[1]published in the Journal of Advances in Modeling Earth Systems (2019), https://doi.org/10.1029/2019MS001847

David Leutwyler[2] and Christoph Schär[2]

[2]Atmospheric and Climate Science, ETH Zürich, Zürich, Switzerland

1. Introduction

Occasionally small waves and vortices appear embedded in the fronts of mid-latitude cyclones. These instabilities draw their energy from gradients in wind speed. Theory describes their formation as a two-stage process (Joly and Thorpe, 1990; Schär and Davies; 1990, Bishop et al., 1999):

1. Deformation and latent heating **strengthen an existing surface front** and thus enable the formation of a narrow low-level sheet of potential vorticity.

2. As the cyclone matures, an eventual **reduction in deformation** favors the instability and may lead to wave-like perturbations along the front, which may grow and break up into a series of vortices.

If the two stages need to be separated in time, why do instabilities sometimes appear in the cores of extratropical cyclones instead of along the front?

2. Hypothesis

The two stages predicted by current theory may co-occur in the same system.
Deformation describes the amount of strain squeezing a front together (frontogenic) or taring it apart (frontolytic) and can be obtained by decomposing the horizontal flow field into its divergent, rotational and deforming contributions (see Schär and Wernli, 1993).

3. Model and Setup

Simulation requires large-scale computational domains and fine resolution to represent the narrow front.

Model:
COSMO 5.0 GPU version (Fuhrer et al., 2018).
We only use the dynamical core and microphysics.

Near-Global Domain:
80° N/S, 360° W/E, 36'000x16'001x60 grid points

Initial Conditions:
Idealized baroclinic wave test (JW, 2006), extended with a moisture profile (Park et al., 2013).

Two 10-day-long simulations :
(1) Δx = 10 km, Δt = 60 s (2) Δx = 1 km, Δt = 6 s

4. Results

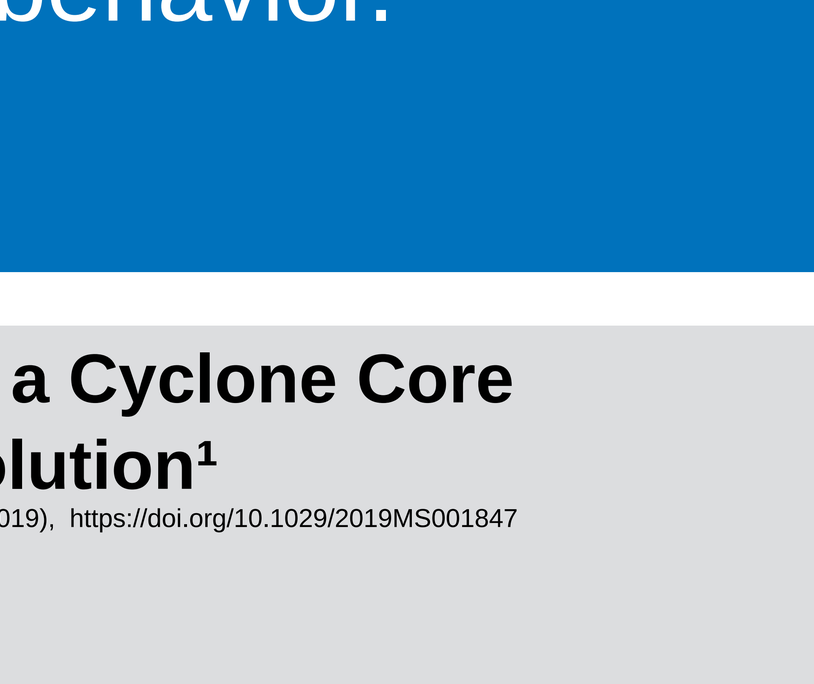

Fig. 1: Deformation (colored shading) along the front of a moist barotropic wave in simulations performed at 10 km and 1 km grid spacing. The black isolines denote surface pressure, the numbers (1 - 13) label meso-vortices identified by eye, and the grey arrows represent deformation vectors pointing in the direction of frontogenesis. For better perceptibly, thedeformation field of the 1 km simulations have been aggregated.

Both phases co-occur along different sections of the elongated cold-front (Fig. 1, top-right panel). Along the south-western portion of the front, strong deformation suppresses the instability (Fig. 1, bottom panel). As the front is advected towards and spirals around the center of the cyclone, active frontogenesis appears to cease (reduction of deformation by one order of magnitude), and the instability emerges. Closer to the cyclone core, the deformation is less prominent, and thus, the instability can grow.

Note also the narrow structure of the deformation zone. Representing this scale collapse accurately appears essential for resolving barotropic instability processes (Fig. 1, top-left panel).

5. Conclusions

Kilometer-scale near-global simulations of idealized baroclinic wave resolve barotropic instability at a cold front.

Limited-area real-case simulation of an observed event confirms the realism of the simulation (see Figures 4 and 5).

Reduced deformation near cyclone core allows secondary barotropic instability to grow.

6. Supplementary Figures

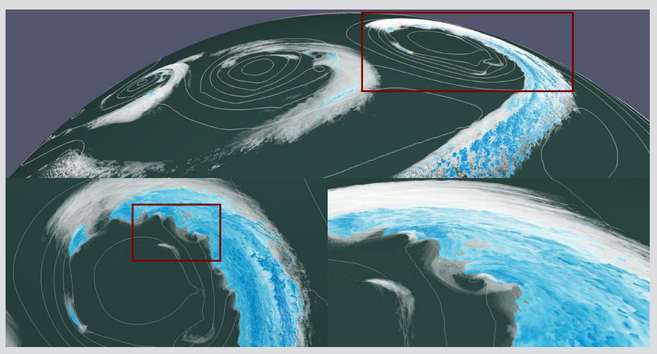

Fig. 2: Perspective view of an idealized moist-baroclinic wave at day 10 of a near-global simulation with 1 km grid spacing and (bottom) meso-vortices embeeded in the frontal system. (White shading) Volume rendering of the sum of cloud ice, cloud water, and graupel and (blue shading) isosurface of rain and snow hydrometeors. (Figures by Tarun Chadha, C2SM)

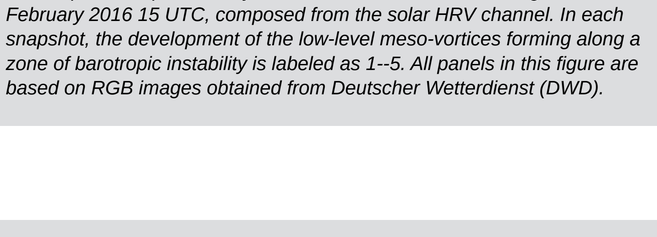

Fig. 3: Zoomed details of vortices embedded in the cold front of the low-pressure system, labeled from 1 - 13. (Left) Precipitation rate, (middle) temperature on the 850 hPa pressure level, and (right) relative vorticity at 10 m height. The black isolines denote surface pressure, with a line spacing of 10 hPa. Note that, for better perceptibly, the vorticity field displayed in the bottom right panel has been aggregated.

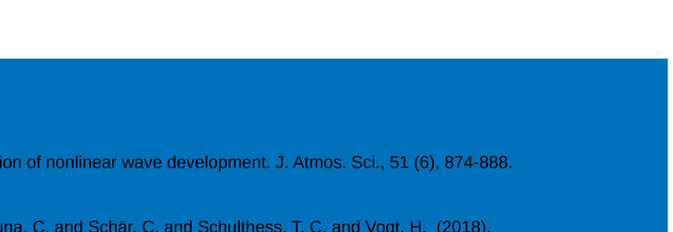

Fig. 4: Snapshots from three SEVIRI/METEOSAT-10 satellite images of an extratropical low-pressure system located Northwest of Portugal on 23 February 2016 15 UTC, composed from the solar HRV channel. In each snapshot, the development of the low-level meso-vortices forming along a zone of barotropic instability is labeled as 1--5. All panels in this figure are based on RGB images obtained from Deutscher Wetterdienst (DWD).

Fig. 5: Simulation of the same system (Fig. 4), driven by ECMWF operational analysis. Each panel contains black contours denoting geopotential height on the 950 hPa pressure level [gpdm] and labels (1 - 4) denoting meso-scale vortices. (Left) The blueish shading denotes vertically-integrated column condensed water. (Middle) The colored shading denotes horizontal wind speed on the 950 hPa pressure level and the white arrows wind vectors. (Right) The colored shading denotes potential vorticity.

References

Bishop, C. H., & Thorpe, A. J. (1994). Frontal wave stability during moist deformation frontogenesis. part ii: The suppression of nonlinear wave development. J. Atmos. Sci., 51 (6), 874-888. doi: 10.1175/1520-0469(1994)051h0874:FWSDMDi2.0.CO;2

Fuhrer, O. and Chadha, T. and Hoefler, T. and Kwasniewski, G. and Lapillonne, X. and Leutwyler, D. and Lüthi, D. and Osuna, C. and Schär, C. and Schulthess, T. C. and Vogt, H. (2018). Near-global climate simulation at 1 km resolution: establishing a performance baseline on 4888 GPUs with COSMO 5.0. Geosci. Model Dev., 11 (4), 1665–1681. doi:10.5194/gmd-11-1665-2018

Jablonowski, C., & Williamson, D. L. (2006). A baroclinic instability test case for atmospheric model dynamical cores. Q. J. Royal Meteorol. Soc., 132 , 2943-2975.

Joly, A., & Thorpe, A. J. (1990). Frontal instability generated by tropospheric potential vorticity anomalies. Q. J. Roy. Meteorol. Soc., 116 (493), 525-560. doi:10.1002/qj.49711649302

Schär, C., & Wernli, H. (1993). Structure and evolution of an isolated semi-geostrophic cyclone. Q. J. Royal Meteorol. Soc., 119 (509), 57-90. doi: 10.1002/qj.49711950904

Schär, C., & Davies, H. C. (1990). An instability of mature cold fronts. J. Atmos. Sci., 47 (8), 929-950. doi: 10.1175/1520-0469(1990)047h0929:AIOMCFi2.0.CO; 2

ETH zürich
Schweizerische Eidgenossenschaft
Confédération suisse
Federal Department of Home Affairs FDHA
Federal Office of Meteorology and Climatology MeteoSwiss

CSCS Centro Svizzero di Calcolo Scientifico Swiss National Supercomputing Centre

C2SM Center for Climate Systems Modeling